International Journal of Computational Methods
(2019) 1950065 (19 pages)

DOI: 10.1142/S0219876219500658

Numerical Simulation of Cracking Process in Rock Mass Under the Coupled Thermo-Mechanical Condition

Xuewei Liu[*,§,¶], Quansheng Liu[†], Jun He[‡] and Fangzheng Yu[†]

[*]*State Key Laboratory of Geomechanics and Geotechnical Engineering*
Institute of Rock and Soil Mechanics, Chinese Academy of Sciences
Wuhan, Hubei, P. R. China

[†]*Key Laboratory of Safety for Geotechnical and Structural Engineering*
of Hubei Province, School of Civil Engineering
Wuhan University, Wuhan, Hubei, P. R. China

[‡]*Key Laboratory of Geotechnical Mechanics and Engineering*
of Ministry of Water Resources
Yangtze River Scientific Research Institute
Wuhan, Hubei, P. R. China

[§]*Department of Civil Engineering, Monash University*
Clayton, VIC, Australia
[¶]*liuxw87@126.com*

Received 1 May 2019
Revised 7 July 2019
Accepted 9 July 2019
Published 1 August 2019

To investigate crack initiation and propagation of rock mass under coupled thermo-mechanical (TM) condition, a two-dimensional coupled TM model based on the numerical manifold method (NMM) is proposed, considering the effect of thermal damage on the rock physical properties and stress on the heat conductivity. Then, the NMM, using empirical strength criteria as the crack propagation critical criterion and physical cover as the minimum failure element, was extended for cracking process simulation. Furthermore, a high-order cover function was used to improve the calculation accuracy of stress. Therefore, the proposed method consists of three parts and has a high accuracy for simulating the cracking process in the rock mass under the coupled TM condition. The ability of the proposed model for high accuracy stress, crack propagation, and thermally-induced cracking simulation was verified by three examples. Finally, the proposed method was applied to simulate the stability of a hypothetical nuclear waste repository. Based on the outcome of this study, the application of NMM can be extended to study rock failure induced by multi-field coupling effect in geo-materials.

Keywords: Numerical manifold method; rock mass; crack propagation; coupled thermo-mechanical; numerical simulation.

[¶]Corresponding author.

1. Introduction

In recent years, the problem of stability in rock mass caused by construction (e.g., geological disposal of nuclear waste, tunnels, enhanced geothermal systems, exploitation of oil, etc.) has emerged as a major challenge. In general, fractured rock mass in a thermal, mechanical, hydraulic, and multi-field coupling environment, and the process of crack initiation and propagation under a coupled multi-field mainly induces rock destruction and collapse. Therefore, understanding the multi-coupling factors and its induced cracking process is significant for both scientific research and engineering application.

The coupled thermo–hydro–mechanical (THM) processes in rock mass have been investigated in detail in the past decades, and significant advances have been achieved. In general, the interaction of coupled TM can be concluded as follows: temperature may decrease both rock strength and elastic modulus and change the stress field; in contrast, the stress may affect the heat conduction coefficient. For example, Zhao *et al.* established a three-dimensional THM coupled model of the fractured media to simulate the extraction of geothermal energy based on a continuum-discrete coupling model [Zhao *et al.* (2015)]. Tang *et al.* discussed the rock mass failure process around a high-level radioactive waste geological disposal repository and established a micromechanical model to describe the rock mass failure process [Tang *et al.* (2007)]. Shen *et al.* proposed a boundary element code on coupled TM processes of rock crack propagation [Shen *et al.* (2013)]. Huang *et al.* applied the discrete element method (DEM) to simulate the random initiation and subsequent propagation in a ceramic nuclear fuel pellet [Huang *et al.* (2014)]. Xia *et al.* proposed a TM coupling particle model based on the particle simulation method and simulated thermally induced rock damage [Xia *et al.* (2014)].

However, most of the above studies treated the fractured rock mass as a continuous material, which cannot consider the effect of crack distribution and propagation on the coupling process. The numerical simulation for the cracking process under coupled TM includes two parts: coupled TM and crack propagation simulation. A large number of studies so far focus on crack propagation simulation, and these methods can be divided into the following two groups: (i) Grid remeshing. This group includes methods such as the traditional FEM [Yang *et al.* (2017); Pal *et al.* (2019)], finite difference method (FDM), and boundary element method (BEM), and their common characteristic is requirement of grid remeshing in every step during crack propagation, including; (ii) does not need grid remeshing. This group includes methods such as DEM [Al-Busaidi *et al.* (2005); Tan *et al.* (2019)], the partition of unity method, discontinuous deformation analysis [Zhao *et al.* (2011)]. Besides, some newly developed numerical methods such as peridynamics [Wang *et al.* (2016, 2018); Wang and Zhou (2019a); Wang *et al.* (2019b)], phase field [Tang *et al.* (2016); Chu *et al.* (2017)], general particle dynamics (GPD) [Zhou and Bi (2018)], which have been proposed for cracking process simulation in rocks. However, some of these methods cannot simulate the full process from

intact to the collapse of rock, and the others may have difficulty simulating the coupled TM.

The numerical manifold method (NMM) was proposed by Shi [1991] and uses two cover systems to simulate the discontinuity between the surfaces of crack, making it possible to simulate cracking process from continuous to discontinuous [Ma *et al.* (2010)]. Therefore, the NMM has been applied in many fracture problems. Zhang *et al.* modeled crack propagation problems containing multiple or branched cracks by the NMM [Zhang *et al.* (2010)]. Wu and Wong [2012] investigated the effects of friction and cohesion on the crack growth from a closed flaw under compression with NMM [Wu and Wong (2012)]. Yang *et al.* developed the NMM to analyze the 3D crack propagation and validated the proposed algorithm with three benchmark problems [Yang *et al.* (2016)]. Liu *et al.* modified the contact model of NMM and proposed NMM for crack initiation and propagation [Liu *et al.* (2017, 2018)].

In recent years, the NMM was extended to study the heat conduction and coupling problems in fractured mass. He *et al.* developed NMM to simulate the thermo-elastic fracturing of rocklike granular materials [He *et al.* (2018)]. Zhang *et al.* proposed the NMM to simulate heat conduction process and the thermal shock cracking [Zhang *et al.* (2017)], and further developed an NMM to solve TM fracture problems [Zhang *et al.* (2014)]. Yang *et al.* proposed coupled hydro-mechanical model with enriched NMM and verified the model with some benchmark problems [Yang *et al.* (2018)]. Liu *et al.* proposed NMM for TH coupling simulation in fractured EGS based on discrete fracture network model [Liu *et al.* (2019a)]. Based on these reports, the application of NMM was extended and enriched. The literature data indicate that most of the studies are focus on the single heat conduction problems, and the coupling and cracking are less considered, and the NMM for simulation of TM coupling is needs further investigation.

In this study, the NMM, including a method and algorithm for coupled TM and crack propagation condition, was extended to simulate the crack initiation and propagation processes under coupled TM condition. The coupled TM governing equation was first used to obtain NMM discretization format, and the corresponding coupling algorithms are presented. Then, the high-order and crack propagation numerical manifold simulation method was proposed. Finally, the proposed method and the numerical approach were validated by four examples.

2. Basic Theory

2.1. *Fundamentals of the NMM*

The most innovative feature of the NMM is two covers, namely mathematical cover (MC) and physical cover (PC), from which the manifold elements (ME) are generated. The MCs are a set of overlapped small patches to cover the problem domain, and the PCs are the intersection of MCs and the physical domain. Obviously, the physical domain is problem dependent. Thus, PCs are a subdivision of MCs in the physical domain, and the ME is the intersection of PCs. In the NMM,

the weight functions are defined by the MC, and the integral area is defined by the MEs.

Then, a cover function (local approximation function) should be defined on each PC to describe the local field characteristic. A convenient way to form a basis of local approximation spaces is polynomial functions, which can be expressed by the following equation [Shi (1991)]:

$$S_c = p(x, y) = \{1, x, y, \ldots, x^n, x^{n-1}y \ldots xy^{n-1}, y^n\} \quad (n = 0, 1, 2 \ldots). \tag{1}$$

Therefore, the local cover function on each PC is defined by the following equation:

$$\begin{Bmatrix} u_i(x, y) \\ v_i(x, y) \end{Bmatrix} = \sum_{j=1}^{m} \begin{Bmatrix} p_{ij}(x, y) & 0 \\ 0 & p_{ij}(x, y) \end{Bmatrix} \begin{Bmatrix} d_{i,2j-1} \\ d_{i,2j} \end{Bmatrix},$$
$$= PD_i \tag{2}$$

where P is polynomial basis shown by Eq. (1), and d_{ij} is the multinomial coefficient.

For different n values, the displacement field can be constant, linear, or other higher order polynomials. A constant cover function with $n = 0$ and higher order functions with $n \geq 1$, can be used to improve the approximation accuracy. In this study, the complete first order cover function is chosen as a local approximation, such that the stress and strain in ME is the first order, and Eq. (2) can be written as the follows:

$$P = \begin{bmatrix} 1 & 0 & x & 0 & y & 0 \\ 0 & 1 & 0 & x & 0 & y \end{bmatrix} \quad D_i = \begin{Bmatrix} d_{i1} \\ d_{i2} \\ d_{i3} \\ d_{i4} \\ d_{i5} \\ d_{i6} \end{Bmatrix} \quad i = 1, 2, 3. \tag{3}$$

The element stiffness matrix, initial stress matrix, loading matrix, and fix point matrix will be changed. For example, the element stiffness matrix can be determined by the following equation:

$$K_{eij} = \iint (B_{ei}^T \cdot E \cdot B_{ej}) dA \quad i, j = 4, 7, 8, \tag{4}$$

where $[E]$ is the elastic matrix and B_{ei} is the strain matrix, which can be given by the following equation:

$$B_{ei} = \begin{bmatrix} \dfrac{\partial}{\partial x} & 0 \\ 0 & \dfrac{\partial}{\partial y} \\ \dfrac{\partial}{\partial y} & \dfrac{\partial}{\partial x} \end{bmatrix} \begin{bmatrix} w_i & 0 & w_i x & 0 & w_i y & 0 \\ 0 & w_i & 0 & w_i x & 0 & w_i y \end{bmatrix}$$

$$= \begin{bmatrix} f_{i2} & 0 & f_{i1} + 2f_{i2}x + f_{i3}y & 0 \\ 0 & f_{i3} & 0 & f_{i3}x \\ f_{i3} & f_{i2} & f_{i3}x & f_{i1} + 2f_{i2}x + f_{i3}y \end{bmatrix}$$

$$\begin{matrix} f_{i2}y & 0 \\ 0 & f_{i1} + f_{i2}x + 2f_{i3}y \\ f_{i1} + f_{i2}x + 2f_{i3}y & f_{i2}y \end{matrix}\Bigg]_{3\times 6} \quad i = 4, 7, 8. \tag{5}$$

Therefore, the element stiffness matrix is an 18×18 order matrix. Furthermore, the local cover functions can be connected together by weight functions to form a global field function on a particular ME. The weight functions depend on the shape of the mathematical mesh, and regular triangular meshes were used in this study. As a result, the weigh functions are same as the three node triangular finite element shape functions.

When the problem domain includes discontinuities, the mathematical meshes first form MCs. Then, the formed MCs and the physical boundaries will define the PCs. If the crack splits a whole MC into two parts, two different PCs will be formed for the same MC located on both sides of the crack. Finally, the NMM elements are generated by these overlapping PCs. Therefore, two different MEs may come from different PCs, but the same MC. As a result, these two MEs will have same weight function but different cover functions, causing different global field function. In this simple way, the discontinuities in the physical domain can fully be captured and described.

2.2. *TM governing equations of rock mass*

Coupled TM governing equations are given as follows [Pan and Feng (2013)]:

$$\begin{cases} kT_{,ii} + Q = \rho c\dot{T}, \\ \sigma_{ij,j} + F_i = 0, \\ \sigma_{ij} = \lambda\varepsilon_{mn}\delta_{ij} + 2G\varepsilon_{ij} - \beta\Delta T\delta_{ij}, \end{cases} \tag{6}$$

where,

$$\beta = K\alpha, \tag{7}$$

$$\lambda = \frac{Ev}{(1+v)(1-2v)}, \tag{8}$$

$$\mu = \frac{E}{2(1+v)}, \tag{9}$$

$$K = 3\lambda + 2\mu = E/(1-2\mu), \tag{10}$$

where σ_{ij} and ε_{ij} are the components of stress and strain, respectively, λ and μ are the lame constants, u is the displacement, F is the body force, T is the temperature, ΔT is the temperature increment, K is the bulk modulus, E is the elastic modulus,

G is the shear modulus, v is the Poisson ratio, k is the coefficient of heat conduction, ρ is the density, α is the coefficient of thermal expansion, c is the specific heat capacity, and Q is the heat source.

The thermal stress would affect the stress field. At the same time, increasing of rock temperature, will change the mechanical properties of the rock mass. In this study, elastic modulus was used to define the damage variable, and the relationship between the temperature and elastic modulus can be expressed as the following equation [Liu and Xu (2000)]:

$$E_T = E_0[1 - F(T)] \tag{11}$$

with

$$F(T) = 6.8 \times 10^{-3} - 1.7 \times 10^{-3}T + 1.07 \times 10^{-5}T^2 - 8.77 \times 10^{-9}T^3, \tag{12}$$

where E_T and E_0 are the elastic modulus at temperature T and 20°C, respectively, $F(T)$ is the thermal impact factor.

Besides, the rock mass thermal conductivity decreases with increasing temperature and increases with increasing axial stress [Görgülü *et al.* (2008)]. The empirical expression for the relationship between the thermal conductivity, temperature, and stress is as follows [Chen *et al.* (2010)]:

$$k = \frac{k_0 + a\sigma^b}{1.007 + (0.0036 - 0.0072/k_0)T}, \tag{13}$$

where k_0 is the initial thermal conductivity, σ is the compressive stress, and a, b are the fitted constant coefficients.

3. NMM for Cracking Process Under Coupled TM

3.1. *NMM for crack propagation*

The first problem is choosing a suitable crack propagation criterion, which can determine the time and occurrence of the new crack. Many critical crack propagation criteria, including maximum circumferential tensile stress, the minimum strain energy release rate, and the maximum energy release rate have been extensively used in literature. However, these criteria can only simulate the cracking process containing pre-existing cracks. To describe the effect of pre-existing cracks and confining pressure on the rock mass strength, Liu *et al.* proposed a new empirical strength criterion described as follows [Liu *et al.* (2017)]:

$$\sigma_1 = \sigma_3 + k_\alpha \sigma_c \frac{1 + A\frac{\sigma_2+\sigma_3}{2\sigma_c}}{1 + B\frac{\sigma_2+\sigma_3}{2\sigma_c}}, \tag{14}$$

where σ_c is the UCS of intact rock, A and B are the constants related to confining pressure. σ_1, σ_2, and σ_3 are the major, intermediate, and minor principal stresses, respectively, and k_α is the adjustment parameter related to the inclination angle α.

When $\sigma_3 < -T_0$ (T_0 is the tensile strength of the intact rock), the tensile failure will be considered first. In the other case, the shear failure will occur when the stress

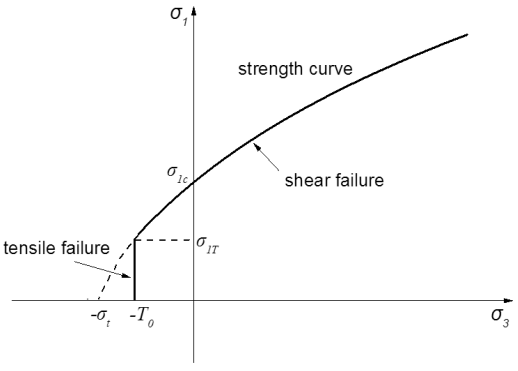

Fig. 1. Strength curve of crack propagation criteria.

state satisfies Eq. (14). Therefore, the final critical criteria for crack propagation is described as follows:

$$\begin{cases} \sigma_3 = -T_0 \\ \sigma_1 = \sigma_3 + k_\alpha \sigma_c \dfrac{1 + A\frac{\sigma_2+\sigma_3}{2\sigma_c}}{1 + B\frac{\sigma_2+\sigma_3}{2\sigma_c}}. \end{cases} \tag{15}$$

The strength curve of new criterion in the local coordinates of $\sigma_1 - \sigma_3$ is shown in Fig. 1, easily indicating that rock tensile and shear propagation modes can be obtained using the improved strength criterion. Therefore, the failure mode can be distinguished by selection the critical criteria during calculation.

Moreover, crack propagation directions were determined as follows: For the tensile failure, the intersection angle between the propagation direction and the minimum principal stress is 90°. For the shearing failure, the intersection angle between the propagation direction and the maximum principal stress can be determined as following:

$$\alpha_1 = \pi/4 + \phi/2, \tag{16}$$

where, the parameter ϕ is the internal friction angle of the intact rock.

The second problem is deciding the crack propagation length during simulation. In this study, the PC is defined as a basic failure element, meaning that the location and orientation of new cracks are determined by the stress state of the PC, and the new crack tip will propagate and stay at the edge of the PC. As a result, the newly formed crack will cut the PC in two parts at every calculation step. However, when two neighboring PCs, which means these two PCs own at least one same ME, satisfying the failure criterion at the same time step, and choosing one will be hard. This problem was solved by two methods, namely the weakest path method and the shortest path method.

The weakest path method is proposed for the situation that arises when the PC without the crack tip satisfies the failure criterion, as shown in Fig. 2. If both of

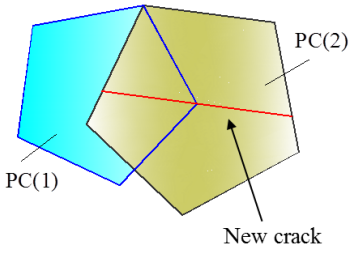

Fig. 2. Illustration of the weakest path and the shortest path methods.

the PCs, namely $PC(1)$ and $PC(2)$, meet the critical conditions, deviatoric stress will be compared first for both of PCs.

$$\Delta\sigma = \sigma_1 - \sigma_3. \tag{17}$$

Then, the newly formed crack will initiate in the PC with the maximum deviatoric stress. As illustrated in Fig. 2, if $(\sigma_1 - \sigma_3)_{PC(2)} \geq (\sigma_1 - \sigma_3)_{PC(1)}$, the new crack will initiate in the PC (2). Furthermore, the new crack is assumed to pass through the center of the PC.

When a PC, containing a crack tip, satisfies the failure criterion, the new crack was assumed to propagate from the crack tip. If the crack tip is in the two PCs at the same time, the shortest path method should be used. As shown in Fig. 3(a), two

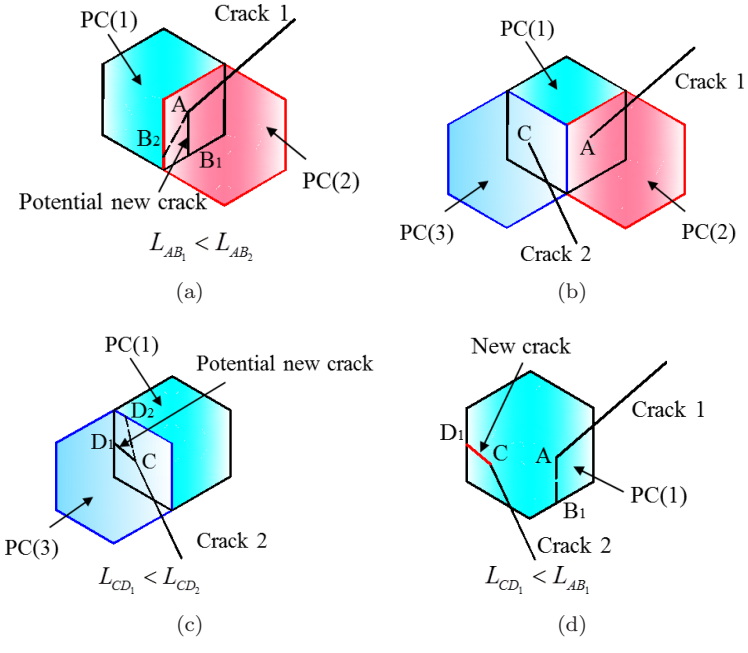

Fig. 3. Illustration of the shortest path method. (a) One crack example. (b) Two cracks example. (c) Crack propagation path for crack 2. (d) Final crack propagation paths.

PCs satisfy the failure criterion, and the potential new crack is in AB_1 and AB_2. The newly formed crack will propagate with the shortest length path, AB_1.

When a PC contains two or more crack tips to satisfy the failure criterion, as illustrated for $PC(1)$ in Fig. 3(b), the shortest path method can still be used assuming the following two steps: first, calculate the whole potential length of new cracks for a certain crack tip according to the simulation results; then, choose the shortest path as the potential new crack for this step. As shown in Figs. 3(a) and 3(c), AB_1 and CD_1 are the potential new cracks for crack tips A and C, respectively. The second step entails comparing the length of all potential new cracks in a certain PC and then choosing the shortest path as the newly formed crack. As shown in Fig. 3(d), there are two potential new cracks in $PC(1)$, and CD_1 is the last newly formed crack.

After the crack initiation and propagation, the new cracks then split the PCs into two or more sub-domains. The PCs and the MEs will be subsequently updated for the next calculation step. Therefore, the effect of crack propagation on the stress and temperature distribution can be represented directly in each step.

3.2. *NMM algorithm*

Numerical manifold method for temperature calculation has been developed, and the NMM discretization format for a transient temperature field can be written by the following equation [Liu and Liu (2013)]:

$$(K + H/\Delta t)D_{n+1} = F + (H/\Delta t)D_n, \tag{18}$$

where K is the whole stiffness matrix, H is the whole heat capacity matrix, Δt is the time increment, D_n is the temperature cover coefficient matrix of the nth step, and F is the whole load matrix.

Crack can affect the rock heat conduction in two different ways: one is prevention of heat conduction and the other is the transfer of heat between rock block. Recent studies indicate that [Liu and Liu (2013)] when the temperature is calculated by the NMM, the discontinuity of temperature field between the two surfaces of crack can be naturally expressed. When a crack prevents heat conduction, the crack will become a part of the heat conduction. In the other instance, the crack will become boundaries. Both of these situations will affect the governing equations and simulation results.

Especially, when considering the effect of heat on an elastic modulus and stress state for crack propagation, the average temperature of the whole problem domain and average stress of every PC should be obtained. The weighted average was used as expressed by the following equations:

$$\overline{T} = \sum_N \frac{\frac{\int_{A_e} T_e dA_e}{A_e}}{N}, \tag{19}$$

$$\overline{\sigma}_P = \frac{\int_A \sigma_e dA_e}{A_e}, \tag{20}$$

Table 1. The algorithm of the proposed method.

1. Meshes generation and parameter initialization
2. Loop for time n
   - 2.1 Estimate the initial rock temperature at time step $T_{w0}^{n} = T_{w}^{n-1}$
   - 2.2 Loop for the TM coupling iteration j
     - a. Obtain the temperature T_{j}^{n} by Eq. (18)
     - b. Calculate damage variable $F(T)$ by Eq. (12) and Eq. (19)
     - c. Calculate stress state
     - d. Calculate thermal conductivity k by Eq. (13)
     - e. Repeat steps a–d
   - 2.3 End TM coupling iteration until convergence criterion is met
   - 2.4 Crack propagation calculation by Eqs. (15) and (20)
   - 2.5 Update crack networks and cover system
   - 2.6 Repeat steps 2.1–2.5 until no new crack generation
3. End loop if the simulation complete

where $\overline{T}$ is the average temperature of the domain, T_e is the temperature distribution of a ME, and N is the amount of the total MEs. The parameter $\overline{\sigma}_P$ is the average stress of a PC, and σ_e is the stress distribution of a ME, and A_e is the area of a ME.

When using the NMM to simulate crack propagation under coupled TM physics, the process can be divided into two modules. The first is the TM solving module, which first establishes a numerical model, considering the thermal effect on the material properties and uses the NMM to obtain the stress and temperature fields. The second module is the crack propagation module, which simulates the crack propagation process. The algorithm for the proposed method is listed in Table 1.

The first step is the generation of meshes and parameter initialization. Then, calculate the temperature distribution $T(x, y)$ according to the boundary conditions, and initial conditions. Furthermore, obtain the average temperature of the whole MEs and calculate the thermal impact factor according to Eqs. (12) and (19), elastic modulus E_T by Eq. (11), and stress distribution. At this time, thermal conductivity k will be calculated by Eq. (13) and the above steps will be repeated until convergence criterion is met. Finally, go to the crack propagation simulation module and modify the PCs and MEs information until no more new crack generated.

4. Numerical Examples

Four numerical examples are presented to verify the capability of the developed method in deformation, cracking propagation under biaxial compression, thermally-induced cracking process, and coupled TM condition simulation.

4.1. *High-order example*

As shown in Fig. 4(a), a cantilever beam is first considered. The parameters of the beam are as follows: length (l), 3 m; height (h), 0.6 m; thickness (b), 1 m; elastic

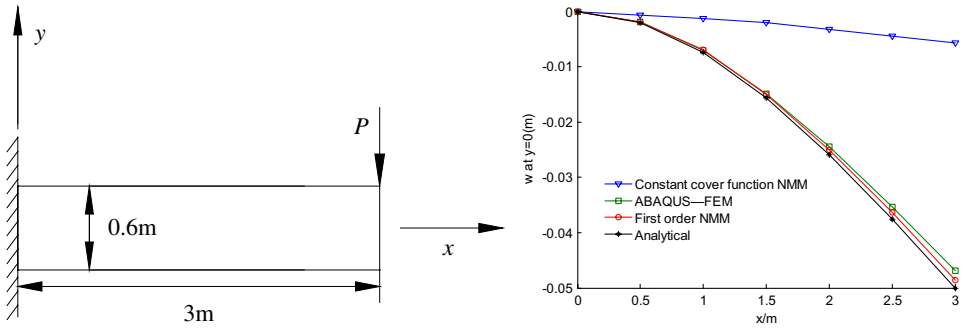

Fig. 4. High-order example. (a) Cantilever beam. (b) Bending deflection under different numerical methods.

modulus (E), 20 GPa; Poisson ratio (v), 0.25. A concentrated force is applied at the right end of the beam, keeping the left side clamped. This example was designed to demonstrate the accuracy of the proposed high-order NMM and calculation codes. The bending deflection of the middle line along the x-axis was compared by different numerical methods. The analytical solution is given by the following equation:

$$w = \frac{Plx^2}{2EI} - \frac{Px^3}{6EI}, \tag{21}$$

where x is the coordinate in x direction.

For the NMM, four different MEs were applied and 360 elements were applied for FEM. Figure 4(b) shows the analytical and numerical solutions, indicating that the complete first order NMM improves the accuracy of the solution compared to that achieved using the constant cover function or FEM.

4.2. *Crack propagation example*

The second example is a biaxial compression test on the rock-like material with an incline crack [Liu *et al.* (2019b)]. As shown in Fig. 5(a), a rectangle plate with length and width are 60 mm and 120 mm, respectively. The boundary conditions are listed as follows: the y directional displacement of bottom is fixed; the left and right sides are applied a confining pressure of 1 MPa and a changed axial pressure is applied on the top boundary. According to the experimental results, the elastic modulus is 1.3 GPa, internal cohesion is 2.44 MPa, internal friction angle is 9.03°, uniaxial compressive strength is 5.45 MPa and tensile strength is 0.9 MPa.

The meshes of NMM and simulated crack propagation paths are shown in Fig. 5(b). The meshes contain 264 physical covers and 462 manifold elements. The experimental result is shown in Fig. 5(c). Compared with Figs. 5(b) and 5(c), it can be found that the crack propagation paths from simulation and test are almost same. Two new cracks were firstly observed to initiate from the two pre-existing crack tips separately and then propagated towards the bottom and top sides of the

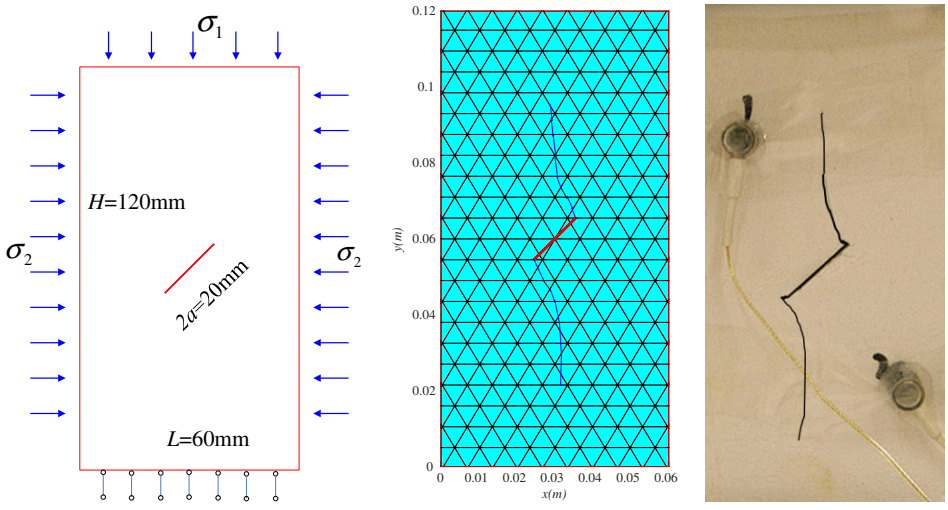

Fig. 5. Crack propagation simulation example. (a) Calculation model. (b) Meshes and crack propagation paths of NMM. (c) Experimental result.

specimen gradually until the final failure. However, the initiation strength for these two methods have some tiny difference. For the numerical simulation, the initiation strength is 3.42 MPa, while this value for the test was 3.20 MPa. The initiation strength of test is lower than that of numerical simulation result. The main reason of this result is that the simulation do not consider the influence of heterogeneous and micro-damage on rock strength. The example in here validates the ability of proposed method on crack propagation simulation.

4.3. *Thermally-induced cracking example*

The crack initiation and propagation process induced by cooling is studied. A rectangle plane with length of 400 mm and high of 200 mm, as shown in Fig. 6(a). The y directional displacement of bottom and x directional displacement of left- and right-hand sides are fixed. The initial temperature in the plane is 1,000°C and the bottom, left, and right surfaces are insulated. The top surface is applied a constant boundary condition with a temperature of 0°C to simulate the cooling circumstance.

The calculation cover system is shown in Fig. 6(b), which contains 598 physical covers and generated 1,098 manifold elements. The simulation model with an elastic modulus of 30GPa, Poisson's ratio of 0.3, initial thermal conductivity of 3.0 W/(m·K) and a coefficient of thermal expansion of $5 \times 10^{-6}(1/°C)$. The uniaxial compression strength is 200 MPa and tensile strength is 10 MPa. The cohesion of rock is 30 MPa, and the internal friction angle is 35°. Parameters a, b are 0.4 and

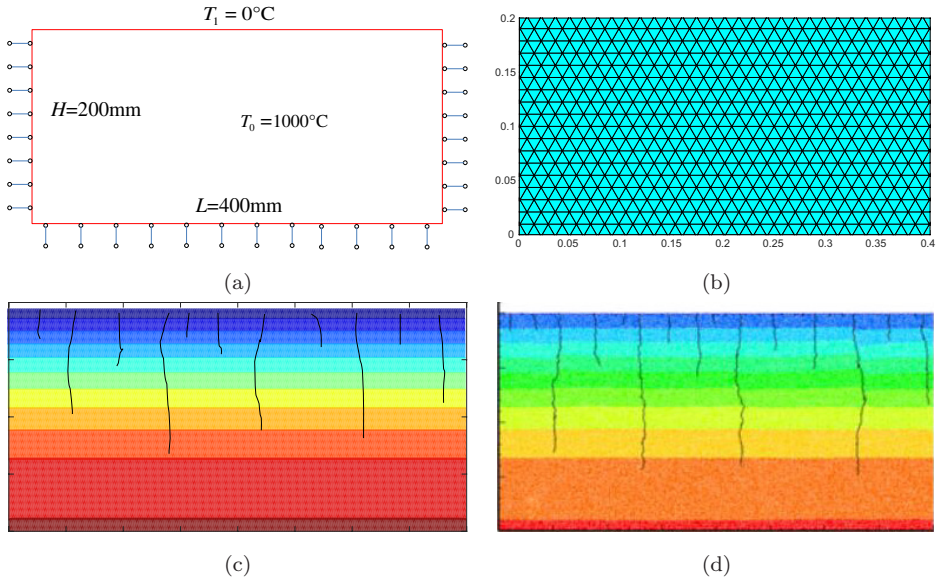

Fig. 6. Thermally-induced cracking example. (a) Calculation model. (b) Meshes. (c) Crack propagation paths and temperature distribution. (d) Literature result [Huang *et al.* (2016)].

0.12. Besides, it is noting that there is no heat conduction across the cracks during calculation.

Figure 6(c) shows the simulation results, indicating that an array of small crack initiated at the top surface firstly due to the thermal contraction. With increase of time, some new cracks stop propagation while others keep growing. Further, most of crack propagates along the direction of temperature gradient and towards the bottom side of plane. Compared with Figs. 6(c) and 6(d), it is clearly that the numerical results in here are agree well with that obtained by Huang *et al.* [2016], which verified the effectiveness of the proposed method on simulation of thermally induced cracking.

4.4. *Hypothetical nuclear waste repository*

A hypothetical nuclear waste repository in intact granite with a laboratory scale was studied. There is a 4 m × 4 m rectangular area with a storage cavern with size of 0.4 m × 0.4 m, as shown in Fig. 6(a). The boundary conditions are as follows: the internal and external surface temperatures are 200°C and 20°C, respectively, whereas the rock initial temperature is 20°C; The displacement of the y direction on the bottom is fixed, while the displacement that in the x direction is fixed on the left- and right-hand sides. There is a vertical downward distributed load on the top with a value of 30 MPa.

Five temperature monitoring points, marked as A, B, C, D, and E, are assigned in the model, as shown in Fig. 7(b), with the coordinates of (0, −0.3 m), (0, −0.5 m),

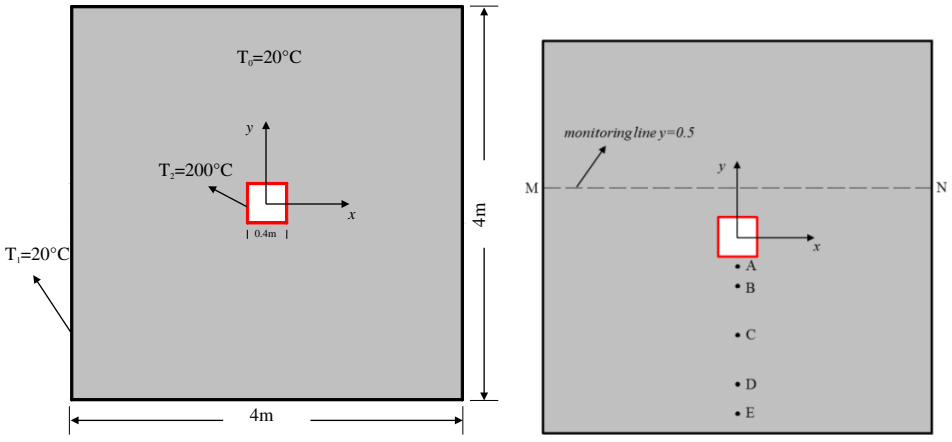

Fig. 7. Simulate model. (a) Boundary conditions. (b) Monitoring line and points.

(0, −1 m), (0, −1.5 m), and (0, −1.8 m), respectively. In addition, a monitoring line (marked as MN) is assigned to monitor the change in the displacement and stress, at a location of $y = 0.5$.

The parameters during the simulation are listed as follows: The density is 2.7 g/cm^3; the elastic modulus of rock at room temperature (20°C) is 70 GPa, while the Poisson's ratio is 0.25; the uniaxial compressive and tensile strength are 200 MPa and 10 MPa, respectively. The cohesion of rock is 30 MPa, and the internal friction angle is 35°. The coefficient of initial heat conduction is 2.7 W/(m · K), parameters a, b in Eq. (13) are 0.4 and 0.12. The coefficient of thermal expansion is 5×10^{-6}(1/°C). The time step used in the simulation of heat conduction is 1d.

Figure 8(a) shows the temperature evolution process at five monitoring points, and the results show that temperature increases rapidly at the beginning and then the slows down gradually until the temperature at points A, B, C, D, and E reached 178.2, 141.9, 84.2, 48.4 and 31.1°C finally. The temperature distribution around the storage cavern is shown in Fig. 8(b), indicating symmetric distribution while no cracks existed in the nuclear waste repository.

Furthermore, the displacement and stress of the monitor line were compared under two conditions. As shown in Fig. 9(a), the displacement in y direction under the thermal influence is lower than that without thermal effect, probably because increasing temperature increases the elastic modulus in this case, thus reducing the displacement. Similarly, the maximum principal stress for two different conditions is compared, as shown in Fig. 9(b). The results show differences in the two conditions. However, it also can be found that the changing of these two parameters have the same tendency under two conditions, indicating that the original distribution characteristics of stress and displacement will not change significantly by the thermal effect.

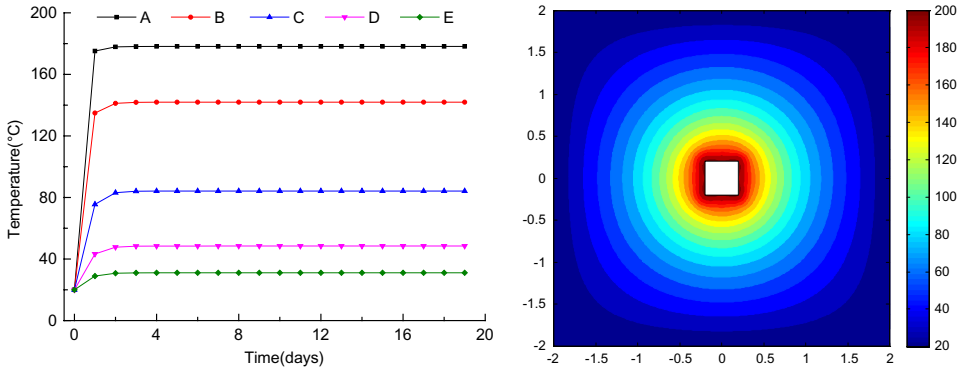

Fig. 8. Temperature results. (a) Temperature versus time at different points. (b) Temperature distribution (Unit: °C).

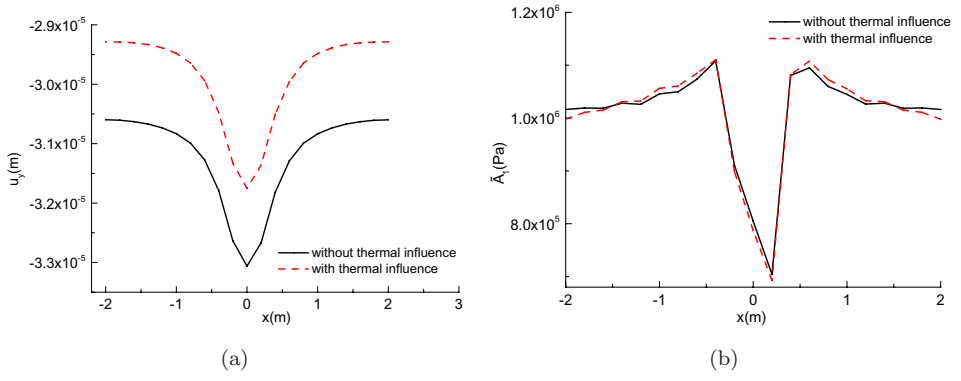

Fig. 9. Calculation results under two different conditions. (a) Displacement in y direction. (b) The maximum principal stress.

Figure 10 shows the stress distribution under single mechanical and coupled TM conditions. Comparing with Figs. 10(a) and 10(b), it is easily found that the stress distribution in the repository changed significantly under the coupled TM. Specially, as shown in Fig. 10(b), the stress in the surrounding rock concentrated, especially at the corner of the floor roof of the cavern. The results indicate that the temperature may affect the original distribution characteristics of the stress field in some content, and can control the stress state sometimes, especially near the region of the heat sources. The results also indicate that the more the change in temperature, more the influence of temperature on stress. These stresses may exceed the tensile strength or shear strength of the rock mass; therefore, cracking around the cavern would occur.

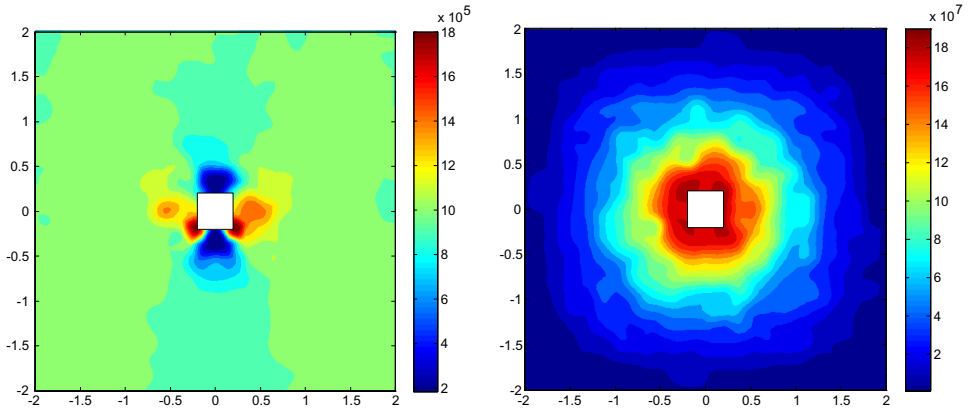

Fig. 10. Comparison of stress distribution under different conditions (Pa). (a) Single mechanical. (b) Coupled TM.

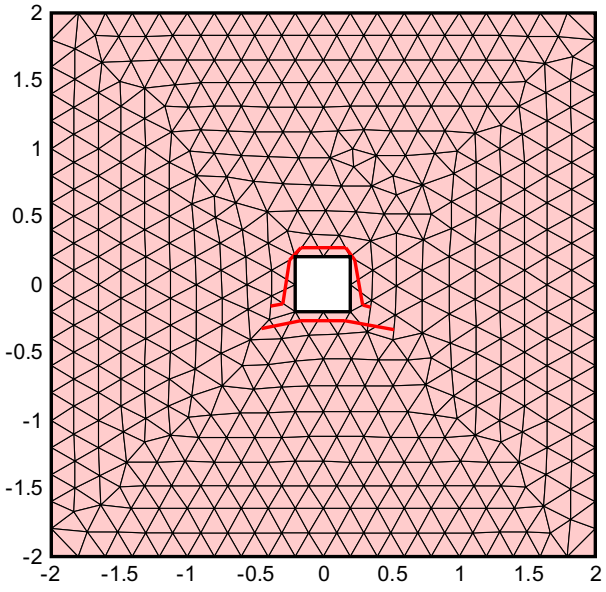

Fig. 11. Predicted rock cracking in repository.

Finally, the crack initiation and propagation process under the coupled TM was calculated. Figure 11 shows distribution of the final cracks in the nuclear waste repository. The results indicate that connected tensile cracks initiated at the roof of the cavern, while a connected crack composing of tensile and shear cracks appeared at a certain depth of the cavern floor. Obviously, the coupled TM affects the stress

and temperature distribution and then changes the crack modes, verifying the effectiveness of the present method as a tool for calculating and predicting cracking induced by a coupled TM process in the rock mass.

5. Conclusion

In conclusion, the NMM was successfully extended to simulate the 2D cracking process under TM coupling. The effects of thermal damage on rock physical properties and stress on heat conductivity were considered in the coupled TM governing equations. Besides, the weighted average method was used to calculate the average temperature of the whole problem domain and average stress of every PC.

Then, the NMM, using empirical strength criteria as the crack propagation critical criterion and physical cover as the minimum failure element, was extended for crack initiation and propagation simulation. A high-order cover function was used to improve the stress accuracy during the calculation. Two principles, namely the weakest path method and the shortest path method, were chosen to decide the place and length of the new cracks formed. Furthermore, the NMM algorithms for cracking and TM coupling simulation were introduced.

The newly developed NMM algorithm was validated by four examples. The first one is a cantilever beam, and the results shows that the complete first-order NMM improved the solution accuracy significantly. The second example was used to check the capability of proposed method on crack propagation simulation under biaxial compression. The third example verified the effectiveness of the proposed method on simulation of thermally induced cracking.

Finally, a hypothetical nuclear waste repository was studied. The results show that the thermal effect on the rock can change the temperature distribution directly and the stress distribution changed immensely at the regions near the heat sources. Due to coupled TM, cracks appeared at a certain depth of the cavern floor and roof. The results in here validated the capability and accuracy of the proposed method.

Acknowledgments

This work was supported by the National Nature Science Foundation of China (Grant Nos. 41602324 and 51774267), and China Scholarship Council (Grant No. 201804910219).

References

Al-Busaidi, A., Hazzard, J. F. and Young, R. P. [2005] "Distinct element modeling of hydraulically fractured Lac du Bonnet granite," *J. Geophys Res. Solid. Earth* **110**, B06302.

Chen, Y. F., Zhou, C. B., Mao, X. Y. and Jing, L. [2010] "Numerical simulation of coupled thermal elastic behaviors for hard rock pillar in Äspö pillar stability experiment, Sweden," *Chin. J. Geotech. Eng.* **32**(8), 1200–1206 (in Chinese).

Chu, D., Li, X. and Liu, Z. [2017] "Study the dynamic crack path in brittle material under thermal shock loading by phase field modeling," *Int. J. Fract.* **208**(1–2), 115–130.

Görgülü, K., Durutürk, Y. S., Demirci, A. and Poyraz, B. [2008] "Influences of uniaxial stress and moisture content on the thermal conductivity of rocks," *Int. J. Rock. Mech. Min. Sci.* **45**(8), 1439–1445.

He, J., Liu, Q., Wu, Z. and Jiang, Y. [2018] "Geothermal-related thermo-elastic fracture analysis by numerical manifold method," *Energies* **11**(6), 1380.

Huang, H., Meakin, P. and Malthe-Sorenssen, A. [2016] "Physics-based simulation of multiple interacting crack growth in brittle rocks driven by thermal cooling," *Int. J. Numer. Anal. Methods Geomech.* **40**(16), 2163–2177.

Huang, H., Spencer, B. and Hales, J. [2014] "Discrete element method for simulation of early-life thermal fracturing behavior in ceramic nuclear fuel pellets," *Nucl. Eng. Design.* **278**, 515–528.

Liu, Q. S. and Xu, X. C. [2000] "Damage analysis of brittle rock at high temperature," *Chin. J. Rock. Mech. Eng.* **19**(4), 408–411 (in Chinese).

Liu, Q. S. and Liu, X. W. [2013] "Preliminary research on numerical manifold method for temperature field of fractured rock mass," *Chin. J. Geotech. Eng.* **35**(4), 635–642.

Liu, X. W., Liu, Q. S., He, J. and Liu, B. [2018] "Modified contact model with rock joint constitutive in numerical manifold method," *Eng. Anal. Bound. Elem.* **93**, 63–71.

Liu, X., Liu, Q., Liu, B., Kang, Y. and He, J. [2019a] "Numerical manifold method for thermal–hydraulic coupling in fractured enhance geothermal system," *Eng. Anal. Bound. Elem.* **101**, 67–75.

Liu, X., Liu, Q., Liu, B., Zhu, Y. and Zhang, P. [2019b] "Failure behavior for rocklike material with cross crack under biaxial compression," *J.Mater. Civil Eng.* **31**(2), 06018025.

Liu, X., Liu, Q., Wei, L. and Huang, X. [2017] "Improved strength criterion and numerical manifold method for fracture initiation and propagation," *Int. J. Geomech.* **17**(5), E4016007.

Ma, G., An, X. and He, L. [2010] "The numerical manifold method: A review," *Int. J. Comput. Methods.* **7**(1), 1–32.

Pal, M. K., Wijerathne, M. L. L. and Hori, M. [2019] "Numerical modeling of brittle cracks using higher order particle discretization scheme–FEM," *Int. J. Comput. Methods* **16**(4), 1843006.

Pan, P. and Feng, X. [2013] "Numerical study on coupled thermo-mechanical processes in Äspö pillar stability experiment," *J. Rock. Mech. Geotech. Eng.* **5**(2), 136–144.

Shen, B., Kim, H. M., Park, E. S., Kim, T. K., Wuttke, M. W., Rinne, M., Backers, T. and Stephansson, O. [2013] "Multi-region boundary element analysis for coupled thermal-fracturing processes in geomaterials," *Rock. Mech. Rock. Eng.* **46**(1), 135–151.

Shi, G. H. [1991] "Manifold method of material analysis," *Trans. 9th Army Conf. Allied Mathematics and Computing*, Minneapolis, USA, 1991, pp. 57–76.

Tan, Y., Zhang, C., Jiang, S. and Feng, Y. T. [2019] "Simulation of ceramic grinding mechanism based on discrete element method," *Int. J. Comput. Methods* **16**(4), 1843008.

Tang, C. A., Ma, T. H., Li, L. C. and Liu, H. Y. [2007] "Rock failure issues in geological disposal of high-level radioactive wastes under multi-field coupling function," *Chin. J. Rock. Mech. Eng.* **26**(S2), 3932–3938 (in Chinese).

Tang, S. B., Zhang, H., Tang, C. A. and Liu, H. Y. [2016] "Numerical model for the cracking behavior of heterogeneous brittle solids subjected to thermal shock," *Int. J. Solid. Struct.* **80**, 520–531.

Wang, Y. T. and Zhou, X. P. [2019a] "Peridynamic simulation of thermal failure behaviors in rocks subjected to heating from boreholes," *Int. J. Rock. Mech. Mining Sci.* **117**, 31–48.

Wang, Y., Zhou, X. and Kou, M. [2019b] "An improved coupled thermo-mechanic bond-based peridynamic model for cracking behaviors in brittle solids subjected to thermal shocks," *Eur. J. Mech.-A/Solid.* **73**, 282–305.

Wang, Y., Zhou, X. and Kou, M. [2018] "Peridynamic investigation on thermal fracturing behavior of ceramic nuclear fuel pellets under power cycles," *Ceramcs. Int.* **44**(10), 11512–11542.

Wang, Y., Zhou, X. and Xu, X. [2016] "Numerical simulation of propagation and coalescence of flaws in rock materials under compressive loads using the extended non-ordinary state-based peridynamics," *Eng. Fract. Mech.* **163**, 248–273.

Wu, Z. and Wong, L. N. Y. [2012] "Frictional crack initiation and propagation analysis using the numerical manifold method," *Comput. Geotech.* **39**, 38–53.

Xia, M., Zhao, C. and Hobbs, B. E. [2014] "Particle simulation of thermally-induced rock damage with consideration of temperature-dependent elastic modulus and strength," *Comput. Geotech.* **55**, 461–473.

Yang, Y., Tang, X., Zheng, H., Liu, Q. and Liu, Z. [2018] "Hydraulic fracturing modeling using the enriched numerical manifold method," *Appl. Math. Model.* **53**, 462–486.

Yang, Y., Tang, X., Zheng, H., Liu, Q. and He, L. [2016] "Three-dimensional fracture propagation with numerical manifold method," *Eng. Anal. Bound. Elem.* **72**, 65–77.

Yang, Y., Zheng, H. and Du, X. [2017] "An enriched edge-based smoothed FEM for linear elastic fracture problems," *Int. J. Comput. Methods.* **14**(5), 1750052.

Zhang, H. H., Li, L. X., An, X. M. and Ma, G. W. [2010] "Numerical analysis of 2D crack propagation problems using the numerical manifold method," *Eng. Anal. Bound. Elem.* **34**(1), 41–50.

Zhang, H. H., Ma, G. W. and Fan, L. F. [2017] "Thermal shock analysis of 2D cracked solids using the numerical manifold method and precise time integration," *Eng. Anal. Bound. Elem.* **75**, 46–56.

Zhang, H. H., Ma, G. W. and Ren, F. [2014] "Implementation of the numerical manifold method for thermo-mechanical fracture of planar solids," *Eng. Anal. Bound. Elem.* **44**, 45–54.

Zhao, Y., Feng, Z., Feng, Z., Yang, D. and Liang, W. [2015] "THM (Thermo-hydro-mechanical) coupled mathematical model of fractured media and numerical simulation of a 3D enhanced geothermal system at 573 K and buried depth 6000–7000 M," *Energy* **82**, 193–205.

Zhao, Z., Zhang, Y. and Bao, H. [2011] "Tunnel blasting simulations by the discontinuous deformation analysis," *Int. J. Comput. Methods* **8**(2), 277–292.

Zhou, X. P. and Bi, J. [2018] "Numerical simulation of thermal cracking in rocks based on general particle dynamics," *J. Eng. Mech.* **144**(1), 04017156.